Next Materials 8 (2025) 100717

Contents lists available at ScienceDirect

Next Materials

journal homepage: www.sciencedirect.com/journal/next-materials

Research article

Effect of hydrothermal aging on the physical, optical and mechanical properties of an experimental 3Y/4Y zirconia bilayer system

Manoela M. Marun [a,*,1,2], Tiago M.B. Campos [a,b,3], Larissa M.M. Alves [a,c,4], Edisa O. Sousa [a,5], Mateus Z. Galli [a,6], Ernesto B. Benalcazar-Jalkh [a,7], Laura F. Carvalho [a,8], Raphaelle S. Monteiro-Sousa [a,9], Edmara T.P. Bergamo [a,10], Sérgio M. Tebcherani [d,11], Petra Gierthmuehlen [e,12], Satoshi Yamaguchi [f,13], Gilmar Patrocinio Thim [g,14], Paulo G. Coelho [h,i,15], Estevam A. Bonfante [a,16]

[a] Department of Prosthodontics and Periodontology, Bauru School of Dentistry – University of São Paulo, Bauru, SP, Brazil
[b] Department of Restorative Dentistry, School of Dentistry, Federal University of Pelotas, Pelotas, RS 96015-560, Brazil
[c] Laboratories for Microstructure Physics & Mechanics of Materials, Department of Preventive and Restorative Sciences, School of Dental Medicine, University of Pennsylvania, Philadelphia, PA 19104, USA
[d] Department of Production Engineering, Federal University of Technology, Ponta Grossa, PR 84016-210, Brazil
[e] Heinrich-Heine-University, Medical Faculty and University Hospital Düsseldorf, Düsseldorf, Department of Prosthodontics, Germany
[f] Department of Dental Biomaterials, Osaka University Graduate School of Dentistry, Suita, Osaka 565-0871, Japan
[g] Laboratory of Plasma and Process, Technological Institute of Aeronautics, Praça Marechal Eduardo Gomes, 50, Vila das Acácias, São José dos Campos, SP 12228-900, Brazil
[h] Division of Plastic Surgery, Miller School of Medicine, University of Miami, Miami, FL 33136, USA
[i] Department of Biochemistry and Molecular Biology, Miller School of Medicine, University of Miami, Miami, FL 33136, USA

ARTICLE INFO

Keywords:
Hydrothermal degradation
Mechanical properties
Zirconia
Ceramics

ABSTRACT

The aim of this study was to synthesize an experimental bilayer zirconia composed of second-generation 3Y-TZP and ultra-translucent 4Y-PSZ, as well as to characterize its microstructure, optical, and mechanical properties, and compare it with its monolithic counterparts before and after hydrothermal aging. Disc-shaped specimens (ISO 6872:2015) were obtained by uniaxial pressing of commercial powders (Zpex and Zpex4; Tosoh Corporation). Then, the discs were sintered at 1550°C for 2 h and divided into 3 groups: bilayer 3Y/4Y, monolithic 3Y and 4Y. Half of the samples of each group were subjected to hydrothermal reactor aging (20 h, 2.2 bar and 134°C). Specimens were characterized using scanning electron microscopy (SEM), X-ray diffraction (XRD) and Raman spectroscopy. Optical properties were determined by contrast ratio (CR) and translucency parameter

* Correspondence to: Alameda Dr. Octavio Pinheiro Brisolla Quadra 9, Brazil
E-mail address: manoela.marun@alumni.usp.br (M.M. Marun).
[1] +55 (14) 996838703
[2] ORCID: 0000–0003-4019–0315
[3] ORCID: 0000–0001-8486–2510
[4] ORCID: 0000–0003-4561–0980
[5] ORCID: 0000–0002-7508–5964
[6] ORCID: 0000–0003 1201–2191
[7] ORCID: 0000–0002-7184–8485
[8] ORCID: 0000–0001-7006–0998
[9] ORCID: 0000–0003-1723–1756
[10] ORCID: 0000–0002-5006–2184
[11] ORCID: 0000–0001-9601–448X
[12] ORCID: 0000–0002-4837–2546
[13] ORCID: 0000–0002-4661–8821
[14] ORCID: 0000–0001-6410–3031
[15] ORCID: 0000–0001-8347–6124
[16] ORCID: 0000–0001-6867–8350

https://doi.org/10.1016/j.nxmate.2025.100717
Received 17 December 2024; Received in revised form 11 April 2025; Accepted 8 May 2025
Available online 16 May 2025

(TP). Mechanical properties were assessed by biaxial flexural strength. XRD evidenced 66 %, 32 %, 66 %, and 40 % of monoclinic phase for aged 3Y-bilayer, 4Y-bilayer, 3Y-control and 4Y-control, respectively. Raman spectra presented monoclinic content on the aged surface of 87 %, 45 %, 87 %, and 47 % for 3Y-bilayer, 4Y-bilayer, 3Y-control, and 4Y-control, respectively. SEM exhibited dense and homogeneous microstructure with smaller grains in bilayer groups, unaffected by aging. Hydrothermal aging did not influence TP and CR, regardless of the system. 3Y demonstrated lower TP and higher CR compared to 4Y and bilayer groups. Aging increased the characteristic strength of all groups. Fractographic marks indicated the origin of fracture and direction of crack propagation from tensile side defects to the compression surface. Hydrothermal aging triggered alterations in the crystalline content, microstructure, and mechanical properties of the experimental bilayer zirconia system as well as of their monolithic controls.

1. Introduction

Polycrystalline yttria-stabilized zirconia (Y-TZP) has been widely used in dentistry due to its biocompatibility, high fracture toughness, and flexural strength [1]. The first generation of zirconia (3Y-TZP) emerged as an aesthetic alternative to metal, replacing the greyish framework appearance for single crowns and fixed dental prostheses (FDPs). It was predominantly composed of tetragonal phase and presented outstanding mechanical properties and high opacity, which demanded the veneering of esthetic porcelain [2,3]. However, due to the high fracture rates of the porcelain veneer material, systematic reviews with long-term clinical studies have advised caution in the recommendation of porcelain fused to 3Y-TZP frameworks for prostheses [4–6].

To overcome these limitations, modifications in the composition, processing and final microstructure of 3Y-TZP were performed to obtain more translucent materials that can be utilized in its monolithic form [7]. Therefore, a significant reduction in the alumina content, and higher sintering temperatures were used to reduce porosities and optimize light transmittance within 3Y-TZP ceramics [7]. However, the slight increase of translucency, made the second zirconia generation esthetically suitable only for posterior areas. Furthermore, the decrease of alumina made the material more susceptible to Low Temperature Degradation (LTD) [8].

The phenomenon of LTD, first described in the 80 s [9], had its clinical impact revealed in orthopedics when 3Y-TZP was introduced for the manufacture of femoral head prostheses in the 1990s. In 2001, a large number of failures occurred in these prostheses due to an accelerated LTD process, raising concerns about the long-term hydrothermal stability of zirconia [10]. This aging occurs when the tetragonal zirconia grains on the surface undergo a phase transformation to monoclinic (stable at room temperature) in the presence of moisture and mechanical stresses, through a mechanism similar to stress corrosion. This process occurs through nucleation and growth, grain by grain, from the surface to the interior of the material. The transformation of a grain leads to volumetric expansion, increasing stresses in adjacent grains and leading to the formation of microcracks due to stress accumulation. These cracks provide a pathway for water penetration into the material. Consequently, grain detachment and increased surface roughness can occur, leading to progressive loss of zirconia's mechanical properties and material fracture [11–13]. Studies have shown the instability of 3Y-TZP *in situ* in a short period of time [14–17] confirming what was demonstrated in the 1980s, [9] and leading to almost abandonment of 3Y-TZP use in orthopedics [18].

In dentistry, a comprehensive series of ex-vivo clinical studies evaluated the development and kinetics of LTD in second-generation zirconia dental prostheses as well as the influence of masticatory mechanical stress on this process over 5 years [14]. It was reported that LTD developed in monolithic restorations of 3Y-TZP six months after intraoral installation and progressed over time. The tetragonal-to-monoclinic phase transformation was not uniform across the material surface, with clusters of transformed grains observed. It was also demonstrated that the phase transformation of unglazed axial areas followed the classic nucleation-growth process reported for LTD, advancing from the surface into the material's bulk. However, in occlusal areas, mechanical stress caused superficial crushing and detachment of transformed grains, leading to an underestimation of the aging process when the evaluation was limited to monoclinic phase quantification. It was also concluded that the presence of glaze at either axial, but especially at the occlusal surface cannot be considered a protection against LTD, as even in areas where the glaze layer was not worn away, tetragonal-to-monoclinic phase transformation was observed. Therefore, long-term analysis of this process is still necessary, as reported results are short to medium-term [14–17].

In the subsequent generations of zirconia, the increase of yttria content (4–5 mol%), led to a significant stabilization of the cubic phase amount. The isotropy of cubic structures improves light transmission, and a significantly higher translucency was achieved. Although materials with predominantly cubic zirconia (5Y-PSZ, ≥50 %c) are less susceptible to LTD [19], the cubic phase does not undergo stress-induced transformation, leading to reduction in fracture resistance and toughness [20]. The following development of 4Y-PSZ resulted in the stabilization of less cubic phase (~25 %c) which maintained high translucency but yielded higher strength (600–1000 MPa) to the material, allowing its indication for posterior 3-unit FDP. Nevertheless, limited information is available regarding the microstructural and mechanical performance of 4Y-PSZ subjected to LTD.

Considering the limitations in previous zirconia generations, multilayered systems were launched in the market, aiming to combine the best properties of each generation, to mimic the translucency gradient of natural teeth without compromising mechanical properties. In general, the clinical indication of multilayered zirconia materials includes crowns (anterior and posterior areas), partial coverage restorations, fixed dental protheses and full-arch prostheses. Moreover, significant differences in zirconia content and composition have been reported among these systems. To ensure proper use, dentists and dental technicians must have a clear understanding of the specific properties of these multilayer materials and it is highly recommended that manufacturer's recommendations are followed [21,22]. Multilayered systems commonly comprise different amounts of cubic phase in each layer, increasing the yttria content from the cervical to the functional occlusal / incisal regions [23]. However, the ideal combination of zirconia powders and the proportion required for specific clinical indications have not been determined by manufacturers. Similarly, differences in the interface composition between layers (blended or not) are present in several commercial systems [22], and the impact of such differences in the mechanical performance of dental prostheses is yet to be determined.

Among different multilayer configurations, the combination of a second-generation 3Y-TZP with an ultra-translucent 4Y-PSZ may result in a favorable balance between high mechanical, improved translucency and reduced susceptibility to LTD regarding pure 3Y-TZP systems due to the higher concentration of cubic phase [24,25]. Therefore, the aim of this study was to synthesize an experimental bilayer zirconia comprised of second-generation 3Y-TZP and an ultra-translucent 4Y-PSZ and to characterize its microstructure, optical and mechanical properties before and after hydrothermal aging compared to its monolithic counterparts (3Y-TZP and 4Y-PSZ). The postulated null hypothesis of the present study was that there would be no significant differences between

the bilayered composition compared to their monolithic controls and that no changes would be detected in the evaluated properties after hydrothermal aging.

2. Material and methods

Disc-shaped specimens were fabricated from commercial zirconia powders comprising the following groups: (i) bilayer 3Y-TZP/4Y-PSZ using commercial 3Y-TZP powder (Zpex, Tosoh Corporation, Tokyo, Japan) and 4Y-PSZ (Zpex4, Tosoh Corporation); (ii) monolithic 3Y-TZP (Zpex); and (iii) monolithic 4Y-PSZ (Zpex4). The composition and particle size of the commercial powders are detailed in Table 1.

For specimen processing, volumetric calculation was performed to determine the necessary amount of each powder to achieve 1.5 mm thick discs to be uniaxially pressed in a tempered steel die with a 15 mm diameter. For bilayers specimen synthesis, the first layer of powder was manual compacted, followed by the second layer, and then the uniaxial pressing was carried out at 3000 kgf/cm^2 (~166 MPa) for 30 seconds, using a hydraulic press (MA098/40 Hydraulic Press, Marconi). Specimens of the control groups were synthesized following the same parameters. All specimens were sintered at 1550°C for 2 hours (LHT 03/17D, Nabertherm Furnace. Lilienthal, Germany) with a heating and cooling rate of 3°C per minute. Half of the samples from each group were subjected to an aging protocol in a hydrothermal reactor (Parr reactor, Parr Instruments, Moline, IL, USA) at 134ºC for 20 hours and 2.2 bars to induce the t-m transformation and simulate the LTD process [26,27].

Specimens for microstructural characterization and optical properties were polished using a semi-automatic polisher (AutoMet 250, Buehler, Lake Buff, IL, USA) with diamond-grid discs up to 1 µm to obtain discs with 1 mm of thickness. The specimens for mechanical testing were not polished to preserve the position of the interface in the middle of the sample, which had final dimensions of Ø12 × ± 1.2 mm (ISO 6872:2015). A schematic representation of the specimens used for each test is represented in Fig. 1.

2.1. Density

The density of sintered specimens (n = 3/group) was calculated using the principle of Archimedes and isopropyl alcohol as the immersion medium. For this purpose, an analytical balance and a theoretical density kit (Analytical balance, Marte Científica, Santa Rita do Sapucaí, MG, Brazil) were employed. To analyze relative density, a theoretical density of 6.07 g/cm^3 was adopted.

2.2. X-ray diffraction (XRD)

X-ray diffraction (XRD) was conducted using a X-Ray diffraction equipment (Model X'pert Powder, PANalytical, Almelo, Holland) to analyze the crystalline content and progression of the t-m transformation due to accelerated aging (n = 3/group). This analysis was performed in both 3Y and 4Y surfaces of the bilayered groups, as well as in 3Y and 4Y monolithic groups, for both immediate and aged conditions. The scan was performed in θ-2θ Bragg geometry, equipped with a graphite monochromator and Cu Kα radiation (λ = 1.5406 Å), operating at a voltage of 40 kV and an emission current of 40 mA. Data were collected over a 2θ range of 20–70° at a scanning rate of 0.2°/minute with a step size of 0.020°. Quantitative phase analysis was carried out using the formulas introduced by Toraya et al. [28] according to the following equations: $Xm = \frac{[Im(-111)+Im(111)]}{[Im(-111)+Im(111)+It(101)]}$, where Im(−111) and Im(111) represent the intensity of the monoclinic peaks (2θ=28° and 2θ=31.2°, respectively) and It(101) indicates the intensity of the tetragonal peak (2θ=30°); and $Vm = \frac{1.311X_m}{(1+0.311X_m)}$, where Vm represents the monoclinic volumetric content.

Additional phase quantification was performed through the formulas presented by Nakamura et al. [29] to determine the amount of transformable tetragonal phase and non-transformable tetragonal and cubic phases.

2.3. Raman

Crystalline spectra of sectioned aged specimens were evaluated using a confocal type Raman spectroscopy equipment (LabRAM HR Evolution, Horiba, Sao Paulo, SP, Brazil). The spectra were recorded between 100 and 750 cm^{-1} with an acquisition time of 30 s, 2 cycles, and a slit size of 100 µm. Measurements were made in sectioned specimens (n = 3/group) at two locations: A) on the surface of the disc and B) 15 µm below at the initial point. Quantitative phase analysis was carried out using the model proposed by Clarke and Adar [30].

2.4. Scanning electron microscope (SEM)

The microstructure was analyzed using a scanning electron microscope with field emission (Tescan Vega3, Libusina, Czech Republic). SEM images were obtained at magnifications of 5000 and 50,000X, on the surface and cross-sectioned view of the specimens and on sectioned samples (n = 2) to evaluate the surface degradation of the grains. Grain sizes were measured from SEM micrographs using the ImageJ software through the Heyn lineal intercept technique [31], with a correction factor of 1.56 applied for tetrakaidekahedral grains [32,33].

2.5. Optical properties

The optical properties were evaluated using the CM 26dG spectrophotometer (Konica Minolta, Tokyo, Japan), which operates in the wavelength range of 360–740 nm. Ten specimens per group were analyzed. In the bilayer specimens' measurements were performed, and data were obtained for both surfaces (3Y and 4Y). Contrast ratio (CR) and translucency parameter (TP) values were obtained from reflectance tests on white background (Yw) and black background (Yb). The contrast ratio (CR) is the property that measures the transparency or opacity of the material and is calculated as the ratio between the reflectance of the specimen on the black background (Yb) and the reflectance of the same specimen on the white background (Yw), given by: $CR = Y_b/Y_w$. The translucency parameter (TP), which determines the material's masking ability, was obtained by calculating the color difference (ΔE) of the specimens on black and white backgrounds according to the following equation: $\Delta E = [(Lb* - Lw*)2 + (ab* - aw*)2 + (bb* - bw*)2]1/2$. Where the L* coordinate represents the lightness of an object. The a* coordinate corresponds to the chromaticity on the red/green axis and b* on the yellow/blue axis. The subscripts b* (black) and w* (white) indicate background color [34–37].

2.6. Biaxial Flexural Strength (BFS)

The biaxial flexural strength test was performed on the specimens (n = 30/group) using the ElectroPulsTM E3000 Linear-Torsion mechan-

Table 1
Characteristics of ceramic powders 3Y-TZP (Zpex) and 4Y-PSZ (Zpex4) according to the manufacturer.

Composition	Zpex	Zpex 4
Y_2O_3 (mol%)	3	4
Actual Particle Size (µm)	0.04 (40 nm)	0.04 (40 nm)
Y_2O_3 (wt%)	5.35 ± 0.2	7.0 ± 0.6
HfO_2 (wt%)	a	< 5.0
Al_2O_3 (wt%)	≤ 0.1	≤ 0.1
SiO_2 (wt%)	≤ 0.02	≤ 0.02
Fe_2O_3 (wt%)	≤ 0.01	≤ 0.01
Na_2O (wt%)	≤ 0.04	≤ 0.06
Pigment (wt%)	-	-
Specific Surface Area (m^2/g)	13 ± 2	16 ± 3

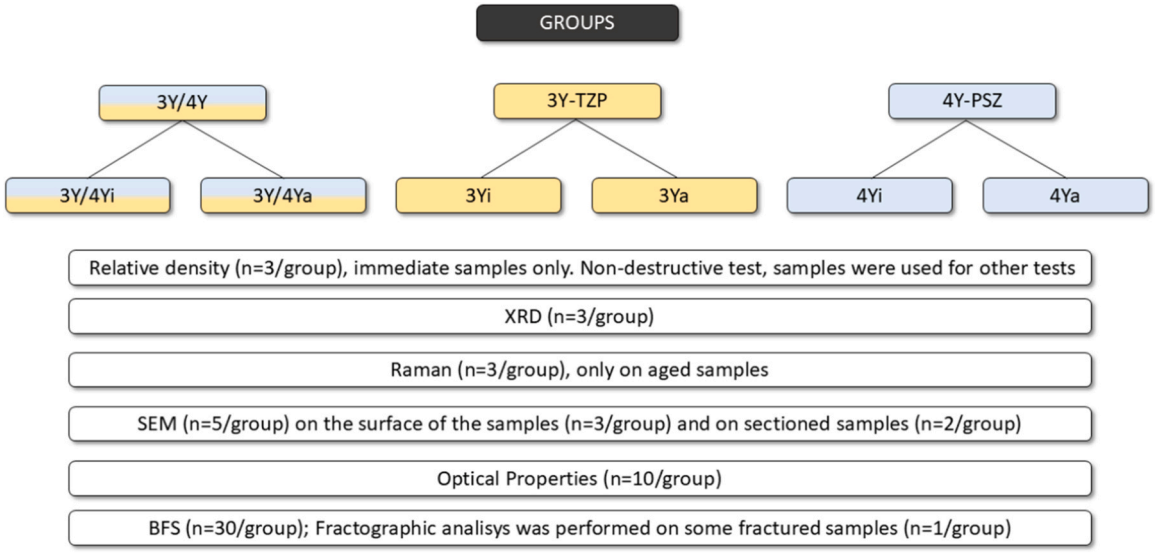

Fig. 1. Schematic representation of the division of groups and the number of specimens used for each test.

ical testing equipment (Instron, Norwood, MA, USA), utilizing a piston-on-three-ball biaxial flexure support, following ISO 6872:2015 standards. The loading rate was 0.5 mm/minute until fracture occurred. The maximum load was recorded for each specimen (N), and the following equations were used to calculate biaxial flexural strength: $\sigma = -0,2387P\left(X - \frac{Y}{b^2}\right)$. Where σ is the biaxial flexural strength, P is the load at fracture (N), b is the specimen thickness at fracture (1.2 ± 0.2 mm), and X and Y are determined by the following equations: $X = (1+\nu)Ln\left(\frac{r_2}{r_3}\right)^2 + \left[\frac{1-\nu}{2}\right]\left(\frac{r_2}{r_3}\right)^2$, and $Y = (1+\nu)\left[1 + Ln + \left(\frac{r_1}{r_3}\right)^2\right] + (1-\nu)\left(\frac{r_1}{r_3}\right)^2$. Where v is the Poisson's ratio (0.31), r_1 is the radius of support circle, r_2 the radius of loaded area, r_3 the radius of specimen, all of these expressed in millimeters [27,38,39].

2.7. Fractographic analysis

Qualitative fractographic analysis was performed on some fractured specimens from the biaxial flexural strength test using an Axio Zoom V16 microscope (Carl Zeiss, Oberkochen, Germany) and a scanning electron microscope with field emission (Tescan Vega3, Libusina, Czech Republic) to identify fractographic marks and confirm the crack origin and direction of propagation.

2.8. Statistical analysis

Data from grain size and optical properties (TP and CR) were tabulated and subjected to descriptive analysis, normality, and homoscedasticity tests. Data normality and homoscedasticity were confirmed using Kolmogorov–Smirnov ($p > 0.05$) and Levene ($p > 0.05$) tests, respectively. Grain size, TP and CR data were statistically evaluated using two-way analysis of variance following post-hoc comparisons by Tukey test, at a significance level of 5 %. The statistical analyses were performed using Minitab software (Minitab, LLC, State College, PA, USA).

The biaxial flexural strength values were subjected to Weibull 2-parameter analysis using (Weibull ++ 22, Reliasoft, Tucson, AZ, USA). A use level probability Weibull was presented to determine probability of failure as a function of stress, and a Weibull 2-parameter contour plot (Weibull modulus [m] vs characteristic strength) was used (95 % confidence intervals) to determine differences between groups. Non-overlap of contour plots indicates a significant difference between them.

3. Results

3.1. Density

The relative density of the sintered specimens according to the Archimedes' principle was above 98 % for all experimental materials (Table 2).

3.2. X-ray diffraction (XRD)

The XRD diffractograms of all groups are depicted in Fig. 2. Characteristic zirconia peaks were identified, and the monoclinic crystalline content quantified. Phase transformation was observed in all groups after aging with the presence of 66 %, 32 %, 66 % and 40 % monoclinic phase, for 3Y-TZP (bilayer), 4Y-PSZ (bilayer), 3Y-TZP (control) and 4Y-PSZ (control), respectively. Additional evaluations allowed the quantification of transformable tetragonal phase, as well as non-transformable tetragonal and cubic phase, presented in Table 3 for all experimental materials in the immediate and aged conditions.

3.3. Raman

Raman spectra (Fig. 3) of aged specimens depicted 87 %; 45 %, 87 % and 47 % monoclinic content on the surface (0 cm^2) of 3Y-TZP (bilayer); 4Y-PSZ (bilayer); 3Y-TZP (control) and 4Y-PSZ (control), respectively. No monoclinic peaks were detected at 15 cm^2 regardless of the material.

3.4. Scanning electron microscope

SEM micrographs (Fig. 4) depicted a dense and homogeneous microstructure, which demonstrates the successful experimental processing protocol with a homogeneous grain distribution. Grains of the

Table 2
Density of sintered discs based on Archimedes' principle.

Material	Density (%)
Bilayer 3Y/4Y	97.89 ± 0.98
3Y-TZP	98.34 ± 0.35
4Y-PSZ	98.82 ± 0.49

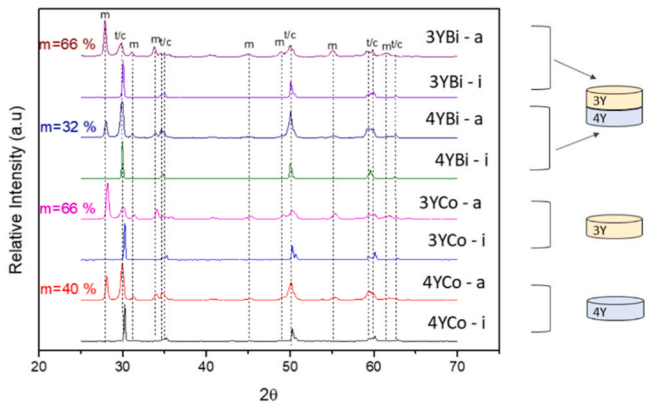

Fig. 2. X-ray diffraction spectra of 3Y-TZP Bilayer (3YBi), 4Y-PSZ Bilayer (4YBi), 3Y-TZP Control (3YCo) and 4Y-PSZ Control (4YCo) Immediate (i) and Aged (a). t: tetragonal, c: cubic and m: monoclinic zirconia phases.

Table 3
Summary of the quantification of monoclinic, transformable tetragonal phase (t) and non-transformable tetragonal (t') and cubic (c) phase for all the experimental groups.

Experimental Group	Monoclinic (m)	Tetragonal (t)	Cubic + Tetragonal' (c + t')
3YBi- i		55.17	44.83
4YBi- i		78.17	21.83
3YBi- a	66	12.17	44.83
4YBi- a	32	23.17	21.83
4YCo - i		55.17	44.83
3YCo - i		78.17	21.83
4YCo - a	40	15.17	44.83
3YCo - a	66	12.17	21.83

bilayer groups were significantly smaller than their respective counterparts. The hydrothermal aging did not affect the surface microstructure and grain size of the specimens from the control and bilayer groups (Table 4). However, in the cross-section analysis presented in Fig. 5, an increase in grain size and along with cluster detachment was observed for control and bilayer groups, being more evident in the 3Y surface for both control and bilayer groups.

3.5. Optical properties

The mean values and standard deviations of the optical properties according to the groups are presented in Table 5. Since there was no statistical difference between the surfaces of the bilayer system (3Y*4Y) ($p > 0.05$), 4Y surface measurements were used in the statistical analysis. Hydrothermal aging did not influence both translucency parameter (TP) and contrast ratio (CR) regardless of the experimental group ($p > 0.05$). Similarly, when comparing 4Y-PSZ bilayer with 4Y-PSZ control under the same aging condition, there is no difference in TP and CR. Whereas, monolithic 3Y demonstrated lower TP and higher CR compared to 4Y-PSZ bilayer and monolithic groups ($p < 0.05$).

3.6. Biaxial flexural strength

Characteristic strength (MPa) and Weibull Modulus (m) are presented in Table 6 as a function of 95 % confidence intervals (CI) before and after aging. Hydrothermal aging significantly increased the characteristic strength of all the experimental groups.

For immediate condition, monolithic 3Y presented higher characteristic strength (1111.50 MPa) than the bilayer system (892.01 MPa) and monolithic 4Y (936.69 MPa). Similar results were observed after aging, where aged monolithic 3Y exhibited higher characteristic strength (1263.66 MPa) compared to 3Y4YA (1061.77 MPa) and aged monolithic 4Y (1140.62 MPa). In both conditions the bilayer group was not statistically different to the 4Y control group. Moreover, no significant differences were observed for Weibull modulus among the experimental groups, with values ranging from 5.7 to 12.8 (Figs. 6 and 7).

3.7. Fractographic analysis

Fractographic marks, including hackle lines (indicating the direction of crack propagation) and compression curls, were observed and used to suggest the origin of the fracture and direction of crack propagation. Fractographic evidence suggested that fractures originated from tensile side defects, which developed during the processing of the ceramic specimens and propagated to the compression side of the samples (Figs. 8 and 9).

4. Discussion

This study proposed the experimental synthesis of a bilayer zirconia system using commercial powder of a second-generation 3Y-TZP and an ultra-translucent 4Y-PSZ and to characterize its microstructure, optical and mechanical properties before and after an accelerated artificial aging protocol to simulate LTD. The bilayer zirconia was also compared with their monolithic 3Y-TZP and 4Y-PSZ counterparts. Since there were statistically significant differences between the control groups and the bilayer group in terms of grain size, translucency parameter, contrast ratio, and characteristic strength, as well as a significant impact of hydrothermal aging in the monoclinic phase composition of the experimental materials, the null hypothesis of the study was rejected.

The relative density values indicated a relative density above 98 % after sintering, regardless of the system. These results are consistent with the SEM micrographs of the immediate specimens, which evidenced a dense surface with uniform grain morphologies and distribution. This corroborates the success of the protocol used for synthesizing the experimental bilayer zirconia system. Further SEM evaluations and grain size depicted significant differences between bilayer and monolithic control groups. Interestingly, the control groups exhibited larger grain sizes than when processed in a bilayer configuration. While 3Y and 4Y control groups presented an average grain size of 1.39 ± 0.24 and 1.92 ± 0.44, respectively, the correspondent 3Y and 4Y surfaces of the bilayer system presented an average grain size of 1.01 ± 0.15 and 1.21 ± 0.18, respectively. The grain sizes of the bilayer group were similar to those reported in a previous study [40], and are in agreement with grain sizes reported for similar sintering temperatures for 3Y and 4Y zirconias [41] since the higher the temperature used for sintering 3Y-TZP, higher grain growth would be expected [20].

To simulate Low-Temperature Degradation (LTD), half of the specimens were subjected to an aging protocol at 134 °C and 2.2 bar in a hydrothermal reactor for 20 hours. This process has been considered an appropriate method for this purpose because promotes an extensive t–m phase transformation (approximately 55–80 % m-phase content) and has been reported to replicate several years of exposure in the oral environment [9,19,26,27,42]. XRD and Raman data quantified the monoclinic phase content in the aged groups, with evidence of a significant tetragonal to monoclinic phase transformation in control and bilayer groups. XRD and Raman depicted t-m phase transformation for 4Y surfaces (bilayer 32 % and 45 %, monolithic 40 % and 47 %, respectively) and as well as for 3Y surfaces (bilayer 66 % and 87 %, monolithic 66 % and 87 %, respectively) after aging. These findings were corroborated by cross-sectioned SEM evaluation, which provides visual evidence of the microstructural degradation of the surface, and are consistent with the existing literature about t-m phase transformation induced by hydrothermal aging, both in 3Y-TZP, which is more susceptible to hydrothermal aging and in 4Y-PSZ, that presents a greater amount of cubic phase (~25 %) [16,21,43,44]. Additionally, in the cross-sectioned SEM micrographs it is possible to observe the

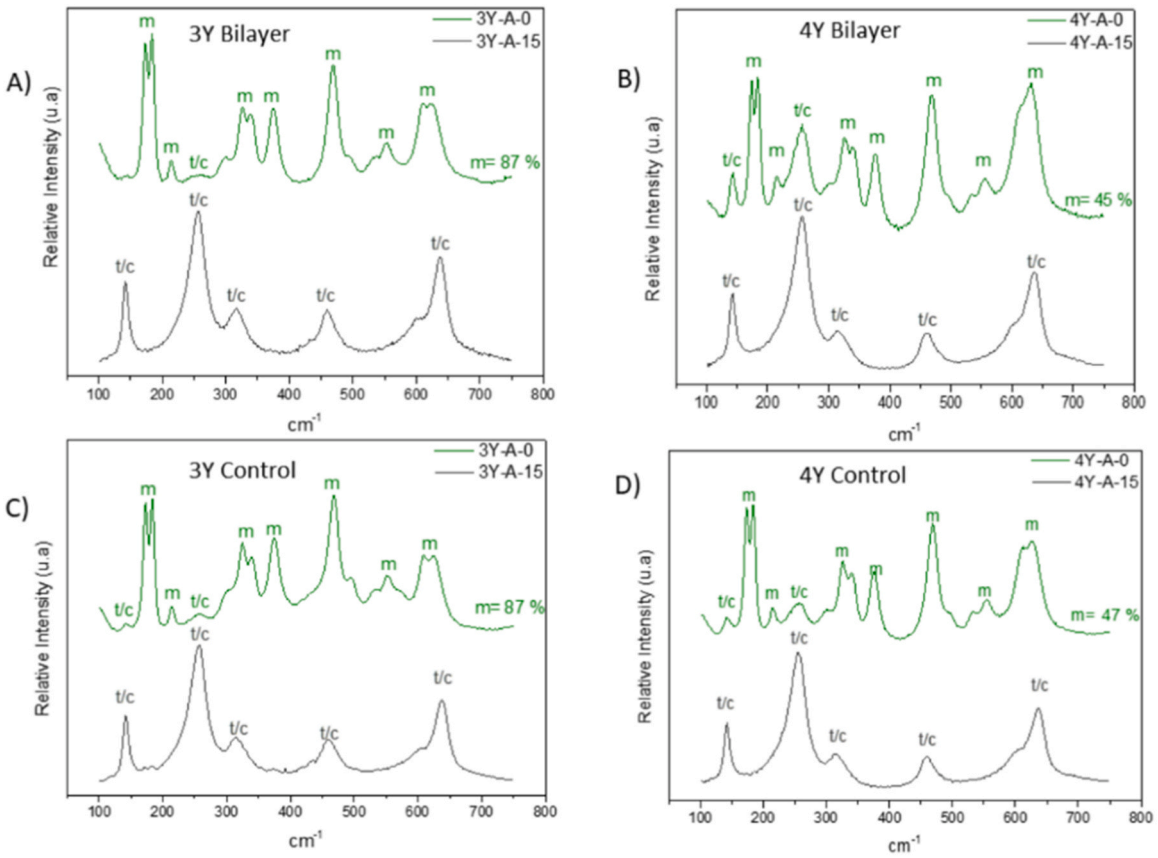

Fig. 3. Raman Spectra of aged specimens. A) 3Y-TZ Bilayer; B) 4Y-PSZ Bilayer. C) 3Y-TZP Control and D) 4Y-PSZ Control. t: tetragonal, c: cubic and m: monoclinic zirconia.

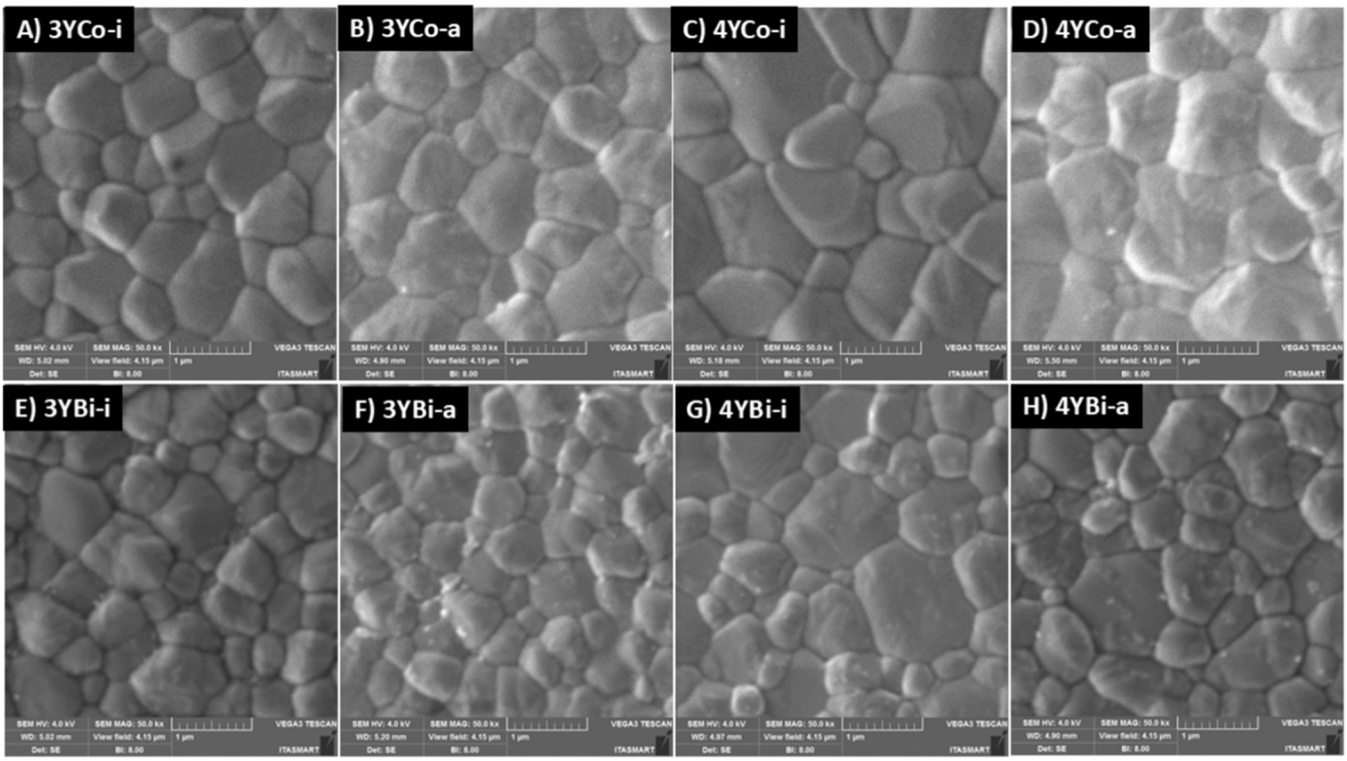

Fig. 4. SEM micrographs of: (A) 3Y-TZP Control immediate, (B) 3Y-TZP Control aged, (C) 4Y-PSZ Control immediate, (D) 4Y-PSZ Control aged, (E) 3Y-TZP Bilayer immediate, (F) 3Y-TZP Bilayer aged, (G) 4Y-PSZ Bilayer immediate and (H) 4Y-PSZ Bilayer aged.

Table 4
Grain size mean and standard deviation (SD) for all groups according to the ceramic system and aging condition and analysis of variance and Tukey Test.

Grain		Size mean (μm) ± SD	
		Immediate	Aged
3Y-TZP	Bilayer	1.01 ± 0.15 Aa	1.04 ± 0.12 Aa
	Control	1.39 ± 0.24 Ba	1.49 ± 0.23 Ba
4Y-PSZ	Bilayer	1.21 ± 0.18 Aa	1.30 ± 0.22 Aa
	Control	1.92 ± 0.44 Ba	1.96 ± 0.41 Ba

Different uppercase letters indicate statistical differences between ceramic systems under the same aging condition. Different lowercase letters indicate statistical differences between aging conditions under the same ceramic system. Comparisons were made for each composition individually.

nucleation and growth process characteristic of low-temperature degradation, occurring grain by grain, from the surface to the interior of the material, leading to volumetric expansion and presenting microcracks in it which has been related to grain detachment and increase surface roughness [11–13,45].

This phenomenon has been described in clinical trials, which suggest that LTD in 3Y-TZP dental prostheses starts within six months of installation and progresses over time, influenced by mechanical stress and occurring even in glazed areas. In occlusal areas, mechanical stress promoted superficial crushing and detachment of transformed grains, leading to an underestimation of the aging process when only monoclinic phase quantification was used. Long-term analysis remains crucial as existing results primarily reflect short to medium-term observations [14–17]. With increasing content of yttrium oxide and higher stabilization of cubic phase, higher aging resistance in zirconia materials would be expected. While the stabilization with 4 mol% of yttrium oxide has been reported to result in higher mechanical properties when compared to 5Y-PSZ [21], 4Y-PSZ is still susceptible to phase transformation, as evidenced by the XRD, Raman, and cross-sectioned imaging presented in this study. Further research is warranted to understand the aging behavior and long-term clinical performance of 4Y-PSZ ceramics.

Although it is claimed that bilayered materials may combine the best properties of each individual monolithic material [46], this was not observed for some properties investigated in the present study. Regarding characteristic strength, under the same aging condition, the bilayer group presented similar strength compared to monolithic 4Y. However, both groups exhibited lower strength compared to monolithic 3Y, regardless of the aging condition. Similar findings have been recently reported for the characterization of experimental bilayer systems comprised of 3Y-TZP and 5Y-PSZ or 4Y-PSZ and 5Y-PSZ, where the characteristic strength of the bilayered systems presented intermediate values compared to their monolithic counterparts [47]. The strength reduction in bilayered systems may be a consequence of the introduction of interfacial defects that produce increased interfacial stress, potentially compromising the material's strength [48,49]. Moreover, the characteristic strength of the bilayered system in this study was comparable to that of experimental bilayers with the same composition, which also exhibited a similar aging behavior [50].

While it has been suggested that flexural strength is negatively

Table 5
Translucency parameter (TP) and Contrast ratio (CR) mean values and standard deviation (SD) for all groups according to the ceramic system and aging condition and analysis of variance and Tukey Test.

	TP mean ± SD		CR mean ± SD	
	Immediate	Aged	Immediate	Aged
4Y-PSZ Bilayer	15.9 ± 0.63 Aa	15.5 ± 0.77 Aa	0.64 ± 0.01Aa	0.65 ± 0.01 Aa
4Y-PSZ Control	16.2 ± 0.4 Aa	15.6 ± 0.55 Aa	0.64 ± 0.008Aa	0.65 ± 0.01 Aa
3Y-TZP Control	14.5 ± 0.43 Ba	14.1 ± 0.54 Ba	0.67 ± 0.008 Ba	0.68 ± 0.01 Ba

Different uppercase letters indicate statistical differences between ceramic systems under the same aging condition. Different lowercase letters indicate statistical differences between aging conditions under the same ceramic system.

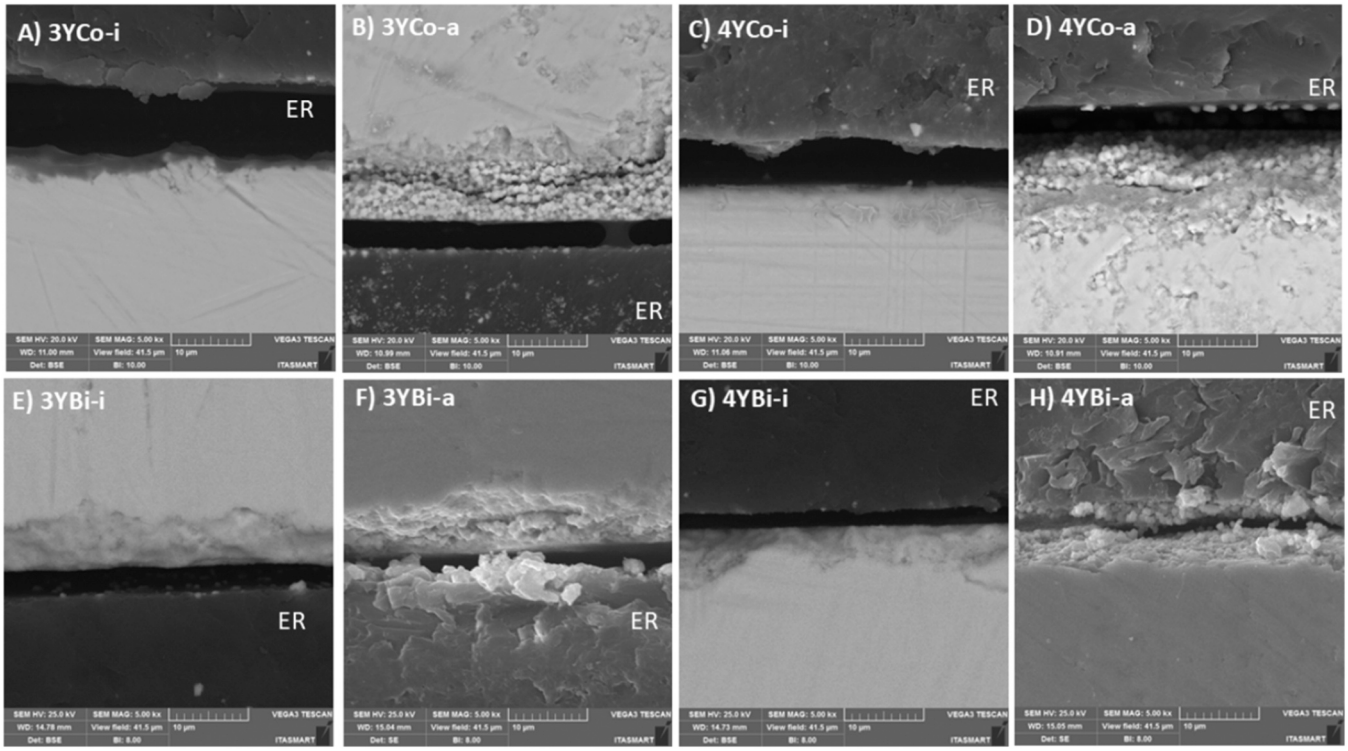

Fig. 5. SEM micrographs of cross-sectioned specimens as follows: (A) 3Y-TZP Control immediate, (B) 3Y-TZP Control aged, (C) 4Y-PSZ Control immediate, (D) 4Y-PSZ Control aged, (E) 3Y-TZP Bilayer immediate, (F) 3Y-TZP Bilayer aged, (G) 4Y-PSZ Bilayer immediate and (H) 4Y-PSZ Bilayer aged. ER: Epoxi resin.

Table 6
Characteristic strength (MPa) and Weibull modulus (m) with their respective upper and lower 95 % confidence bounds for immediate and aged groups.

CI: 0.95	3Y4Y I	3Y4Y A	3Y I	3Y A	4Y I	4Y A
Upper	937.86	1099.73	1164.17	1301.11	1000.63	1184.73
Characteristic strength (MPa)	**892.01 Aa**	**1061.77Ab**	**1111.50 Ba**	**1263.66Bb**	**936.69Aa**	**1140.62Ab**
Lower	848.38	1025.13	1061.22	1227.28	876.84	1098.16
Upper	9.85	14.21	10.66	17.26	7.62	13.06
Weibull modulus (m)	**7.54 Aa**	**10.64 Aa**	**8.13 Aa**	**12.84 Aa**	**5.70 Aa**	**9.97 Aa**
Lower	5.76	7.97	6.2	9.56	4.27	7.61

Uppercase letters represent statistical differences between materials under the same condition. Lowercase letters indicate statistical differences for the same material before and after aging.

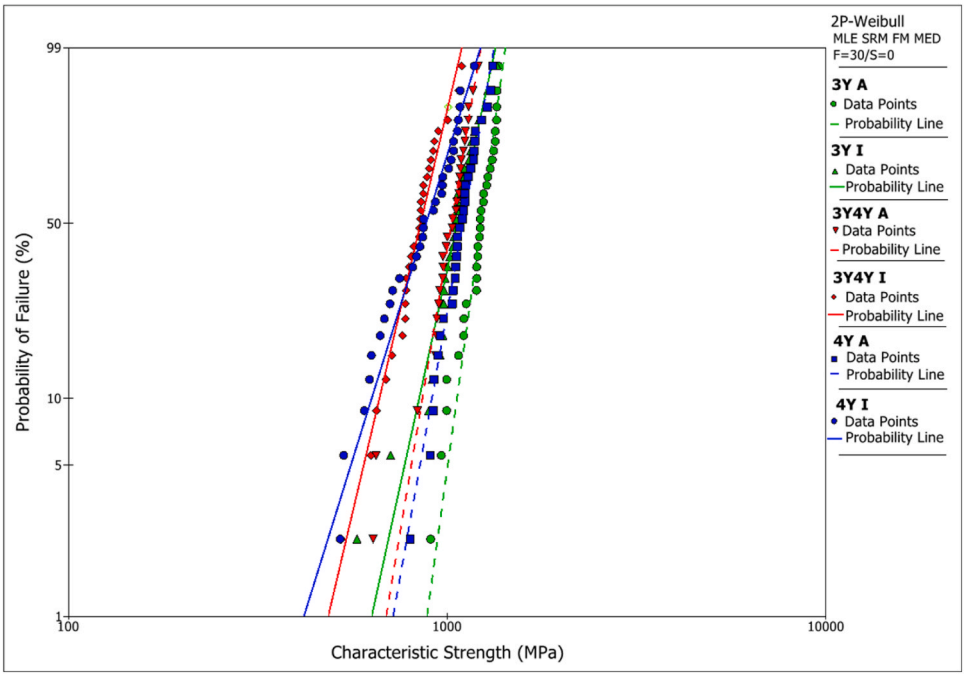

Fig. 6. Use level probability Weibull curves, showing the probability of failure as a function of characteristic strength (MPa).

affected when at least 50 % of m-phase is detected on the material's surface [27], in the present study aging significantly increased the characteristic strength of all the experimental groups. These findings may be explained by the transformation toughening mechanism characteristic of 3Y-TZP ceramics, also present in 4Y-PSZ. The t-m phase transformation has been associated with a 3–4 % volumetric expansion, which generates compressive stress concentration around defects, and may hinder crack propagation increasing strength and fracture toughness [42]. Furthermore, it has been suggested that despite surface changes, nanomechanical properties remain preserved below the surface and at the interface of bilayered zirconias after aging, which might also explain the absence of deleterious effects in strength after hydrothermal aging [40].

Additionally, no significant difference was observed in the Weibull modulus among the groups, indicating that there was no decrease on the material's structural reliability. In fact, aging did not negatively affect the reliability of the materials. Previous studies have shown that some aging protocols increase Weibull modulus compared to immediate counterparts, likely due to zirconia's toughening mechanism that prevents crack propagation [42,51].

Regarding the outcomes for optical properties, hydrothermal aging did not affect the translucency parameter (TP) and contrast ratio (CR) of the experimental groups. However, under the same aging condition, significant differences for TP and CR were observed between 3Y control, 4Y control and bilayer groups. As expected, monolithic 4Y exhibited higher TP and lower CR values compared to monolithic 3Y, whereas, even with a 3Y layer, the bilayer system presented similar translucency and contrast ratio of monolithic 4Y, demonstrating the effectiveness of synthesizing bilayer system without jeopardizing light transmittance. The optical parameters of monolithic second-generation zirconia are limited due to the natural opacity of the birefringent tetragonal crystals, which causes light scattering within the material's structure [21,52].

Fractographic analysis revealed hackle lines and compression curls, indicating that the fracture originated from tensile side defects developed during ceramic specimen processing and from the artificial aging process, and propagated to the compression side of the disc, as previously reported [53,54]. At the fractographic evaluation, no important features were observed in the boundary region between 3Y and 4Y, suggesting a smooth transition between both layers. To synthesize multilayer materials, the common approach consists in incrementally pressing different powder compositions. However, this method has been associated with the formation of interfacial defects, such as impurities or poorly sintered regions, which make the interfaces more prone to fracture [55]. In fact, weaker interfaces between chromatic layers have been reported regarding the interfacial strength of commercial multichromatic systems, where a lower failure stress has been observed at the multilayer region (~30 %) compared to the enamel or dentin counterparts [55]. These findings may also be accompanied by the formation of residual stress and explain the significantly lower resistance observed for the bilayer system regarding the 3Y control group.

The synthesis of the experimental bilayered system present some limitations, including the absence of isostatic pressing and pre-sintering

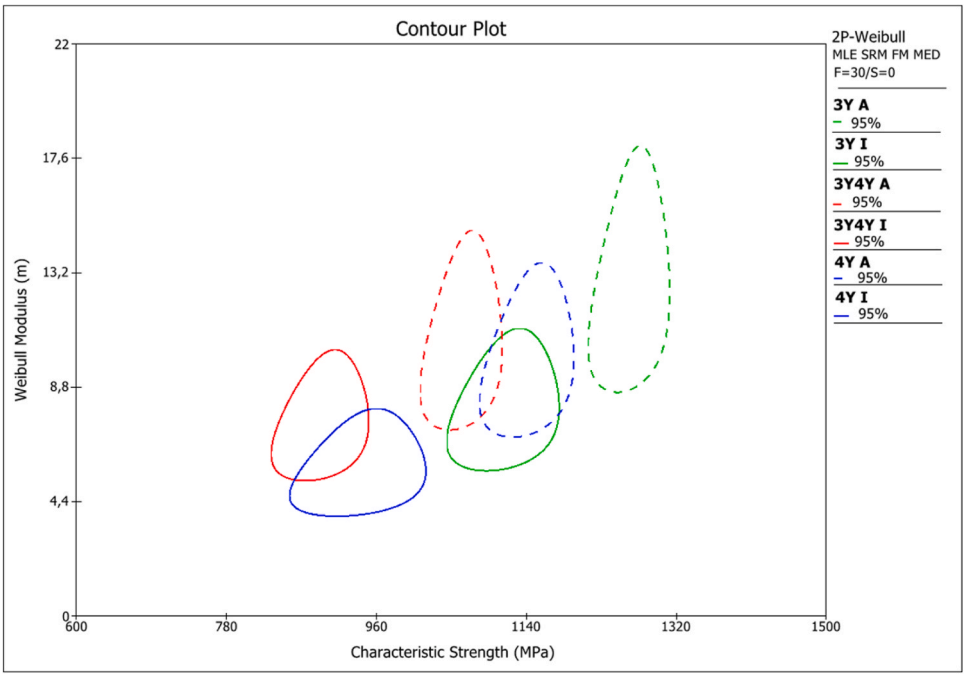

Fig. 7. Contour plot showing the relationship between Weibull modulus (m) and characteristic strength (MPa). The nonoverlap between contours indicates statistically significant difference.

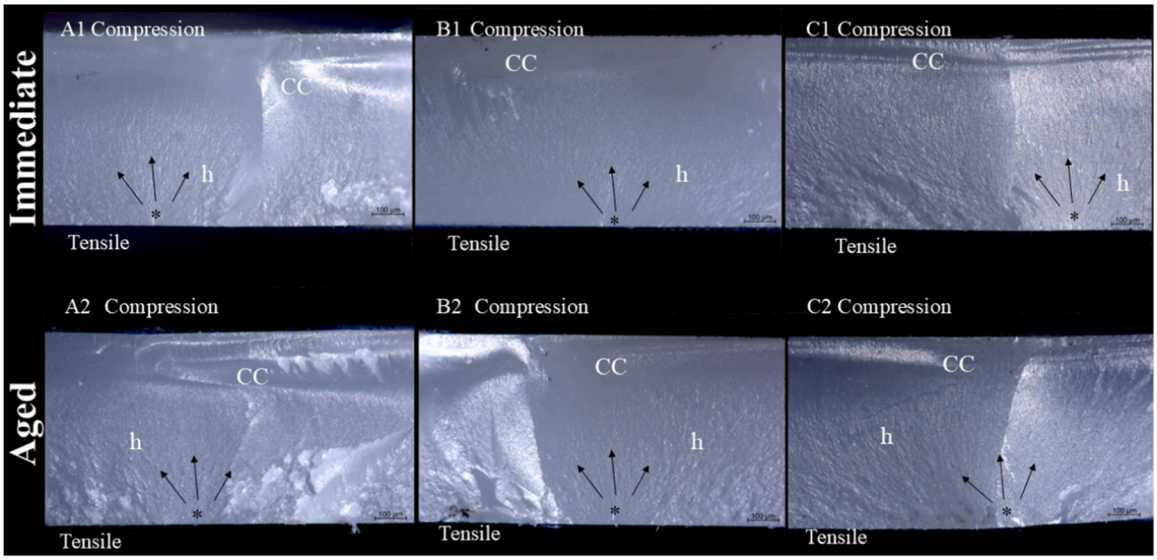

Fig. 8. Stereomicroscope micrographs of fractured surfaces of 3Y-TZP/4Y-PSZ Bilayer (A), 4Y-PSZ Control (B), 3Y-TZP Control (C), before (A1, B1, and C1, respectively) and after aging (A2, B2, and C2, respectively). Compression curl (CC), hackle lines (h) and failure origin (*) are depicted in the images with 200x magnification. The CC denote the surface under compression and suggest the fracture origin to be placed in the opposite surface. In the facture surface, hackle lines indicate the direction of fracture propagation, suggesting the presence of the fracture origin in the tensile side of the samples.

process as performed for commercial zirconia pucks. It is unknown whether these differences may or may not have a significant impact on the microstructure and overall properties compared to commercial multilayer systems. Additionally, the hydrothermal aging conditions do not fully replicate the complex in vivo degradation mechanisms and do not account for the repeated occlusal forces of the oral environment. Therefore, future research should focus on fatigue testing and long-term clinical studies to further validate the findings of the present study.

5. Conclusion

The synthesis of the bilayer system resulted in a dense and homogeneous microstructure. Hydrothermal aging triggered alterations in the crystalline content, microstructure, and mechanical properties of the experimental bilayer zirconia system as well as of their monolithic controls.

Funding

This study was supported by the São Paulo Research Foundation

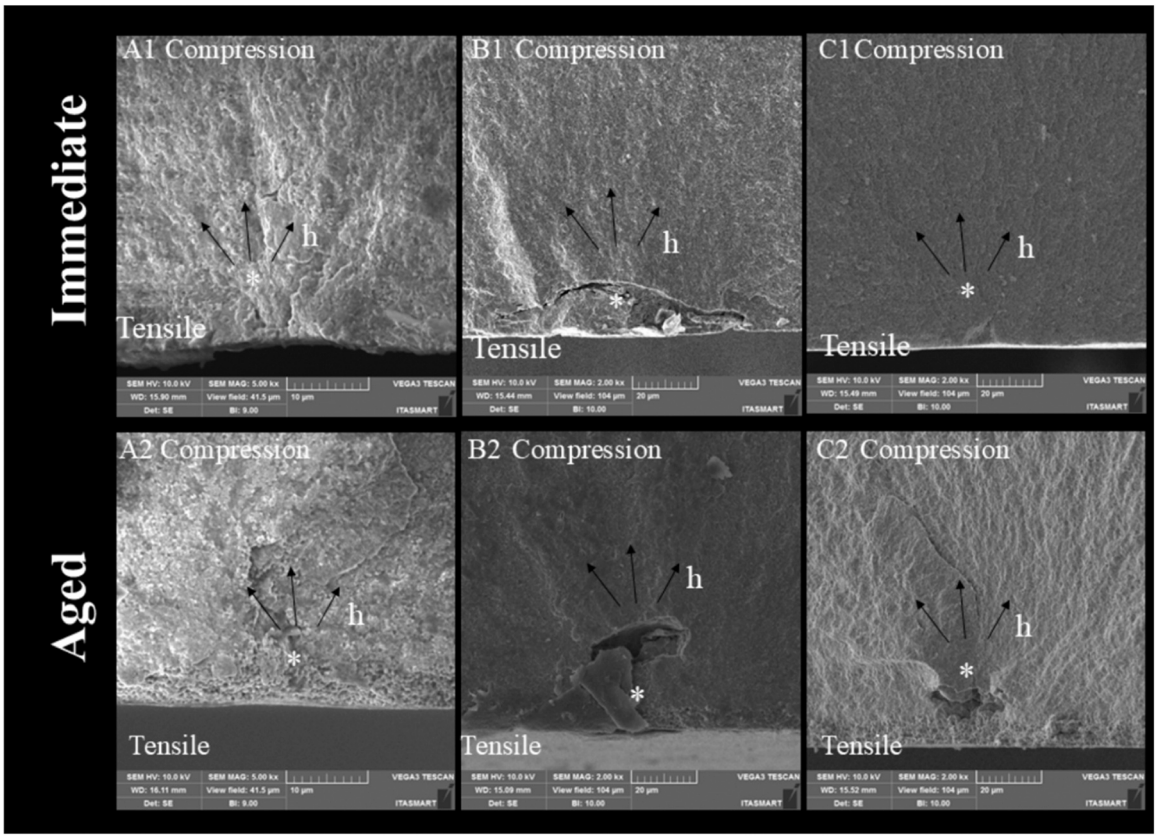

Fig. 9. SEM micrographs of fractured surfaces of 3Y-TZP/4Y-PSZ Bilayer (A), 4Y-PSZ Control (B), 3Y-TZP Control (C) before (A1, B1, and C1, respectively), and after aging (A2, B2, and C2, respectively). Hackle lines (h) suggest the direction of crack propagation (arrows) and failure origin (*).

(FAPESP), grants nos. 2021/06730–7, 2022/05496-3, 2022/05495-7, 2022/07733–2, 2023/02142–9, 2021/07440–2, 2023/07289–8, 2018/03072–6, 2019/00452–5, 2020/12874–9, 2023/08712, 2019/08693–1, 2022/07157-1 and 2021/08018–2. Additionally, funding was provided by the National Council for Scientific and Technological Development (CNPq) grant no. 307255/2021–2. This study was financed in part by the Coordenação de Aperfeiçoamento Pessoal de Nivel Superior – Brasil (CAPES) Finance Code 001; 88887.696690/2022–00. The authors are also thankful to Laboratory of Plasma and Processes (LPP) at Technological Aeronautical Institute.

CRediT authorship contribution statement

Manoela Medola Marun: Writing – Acquisition and interpretation of data, original draft, and final approval of the submitted version; **Tiago M. B. Campos:** conception and design of the study, critical revision of the original draft, and final approval of the submitted version. **Larissa M.M. Alves:** Interpretation of data, critical revision of the original draft, and final approval of the submitted version. **Edisa O. Sousa:** data acquisition, writing the original draft, and final approval of the submitted version. **Mateus Z. Galli:** data acquisition, writing the original draft, and final approval of the submitted version. **Ernesto B. Benalcazar-Jalkh:** Interpretation of data, critical revision of the original draft, and final approval of the submitted version. **Laura F. Carvalho:** data acquisition, writing the original draft, and final approval of the submitted version. **Raphaelle Santos Monteiro:** data acquisition, writing the original draft, and final approval of the submitted version. **Edmara T.P. Bergamo:** Interpretation of data, critical revision of the original draft, and final approval of the submitted version. **Sérgio M. Tebcherani:** Interpretation of data, critical revision of the original draft, and final approval of the submitted version. **Petra Gierthmuehlen:** Interpretation of data, critical revision of the original draft, and final approval of the submitted version. **Satoshi Yamaguchi:** Conception and design of the study, critical revision of the original draft, and final approval of the submitted version. **Gilmar Patrocínio Thim:** Conception and design of the study, critical revision of the original draft, and final approval of the submitted version. **Paulo G. Coelho:** Conception and design of the study, critical revision of the original draft, and final approval of the submitted version. **Estevam A. Bonfante:** Conception and design of the study, data interpretation, critical revision of the original draft, and final approval of the submitted version. All authors agree to be accountable for all aspects of the work in ensuring that questions related to the accuracy or integrity of any part of the work are appropriately investigated and resolved.

Declaration of Competing Interest

The authors declare that they have no known competing financial interests or personal relationships that could have appeared to influence the work reported in this paper.

References

[1] P. Shelar, H. Abdolvand, S. Butler, On the behaviour of zirconia-based dental materials: A review, J. Mech. Behav. Biomed. Mater. 124 (2021) 104861, https://doi.org/10.1016/j.jmbbm.2021.104861.
[2] E.B. Benalcazar Jalkh, K.N. Monteiro, P.F. Cesar, L.A. Genova, E.T.P. Bergamo, A.C. de O. Lopes, et al., Aging resistant ZTA composite for dental applications: Microstructural, optical and mechanical characterization, Dent. Mater. 36 (2020) 1190–1200, https://doi.org/10.1016/j.dental.2020.05.011.
[3] S. Gracis, V. Thompson, J. Ferencz, N. Silva, E. Bonfante, A new classification system for all-ceramic and ceramic-like restorative materials, Int J. Prosthodont 28 (2016) 227–235, https://doi.org/10.11607/ijp.4244.
[4] M. Balmer, M. Payer, R.-J. Kohal, B.C. Spies, EAO position paper: current level of evidence regarding zirconia implants in clinical trials, Int J. Prosthodont 35 (2022) 560–566, https://doi.org/10.11607/ijp.8131.

[5] S. Pieralli, R. Kohal, K. Rabel, M. Von Stein-Lausnitz, K. Vach, B.C. Spies, Clinical outcomes of partial and full-arch all-ceramic implant-supported fixed dental prostheses. A systematic review and meta-analysis, Clin. Oral. Implants Res 29 (2018) 224–236, https://doi.org/10.1111/clr.13345.

[6] B.E. Pjetursson, I. Sailer, E. Merino-Higuera, B.C. Spies, F. Burkhardt, D. Karasan, Systematic review evaluating the influence of the prosthetic material and prosthetic design on the clinical outcomes of implant-supported multi-unit fixed dental prosthesis in the posterior area, Clin. Oral. Implants Res 34 (26) (2023) 86–103, https://doi.org/10.1111/clr.14103.

[7] Y. Zhang, B.R. Lawn, Novel zirconia materials in dentistry, J. Dent. Res 97 (2018) 140–147, https://doi.org/10.1177/0022034517737483.

[8] S.M. Fathy, A.A. El-Fallal, S.A. El-Negoly, A.B. El Bedawy, Translucency of monolithic and core zirconia after hydrothermal aging, Acta Biomater. Odontol. Scand. 1 (2015) 86–92, https://doi.org/10.3109/23337931.2015.1102639.

[9] K. Kobayashi, H. Kuwajima, T. Masaki, Phase change and mechanical properties of ZrO2-Y2O3 solid electrolyte after ageing, Solid State Ion. 3–4 (1981) 489–493, https://doi.org/10.1016/0167-2738(81)90138-7.

[10] J. Chevalier, What future for zirconia as a biomaterial? Biomaterials 27 (2006) 535–543, https://doi.org/10.1016/j.biomaterials.2005.07.034.

[11] J. Chevalier, What future for zirconia as a biomaterial? Biomaterials 27 (2006) 535–543, https://doi.org/10.1016/j.biomaterials.2005.07.034.

[12] J. Chevalier, L. Gremillard, Ceramics for medical applications: a picture for the next 20 years, J. Eur. Ceram. Soc. 29 (2009) 1245–1255, https://doi.org/10.1016/j.jeurceramsoc.2008.08.025.

[13] M. Keuper, C. Berthold, K.G. Nickel, Long-time aging in 3mol.% yttria-stabilized tetragonal zirconia polycrystals at human body temperature, Acta Biomater. 10 (2014) 951–959, https://doi.org/10.1016/j.actbio.2013.09.033.

[14] V. Koenig, C.P. Wulfman, M.A. Derbanne, N.M. Dupont, S.O. Le Goff, M.-L. Tang, et al., Aging of monolithic zirconia dental prostheses: protocol for a 5-year prospective clinical study using ex vivo analyses, Conte Clin. Trials Commun. 4 (2016) 25–32, https://doi.org/10.1016/j.conctc.2016.06.001.

[15] V. Koenig, C. Wulfman, S. Bekaert, N. Dupont, S. Le Goff, M. Eldafrawy, et al., Clinical behavior of second-generation zirconia monolithic posterior restorations: two-year results of a prospective study with Ex vivo analyses including patients with clinical signs of bruxism, J. Dent. 91 (2019) 103229, https://doi.org/10.1016/j.jdent.2019.103229.

[16] V. Koenig, S. Bekaert, N. Dupont, A. Vanheusden, S. Le Goff, T. Douillard, et al., Intraoral low-temperature degradation of monolithic zirconia dental prostheses: results of a prospective clinical study with ex vivo monitoring, Dent. Mater. 37 (2021) 1134–1149, https://doi.org/10.1016/j.dental.2021.03.008.

[17] V. Koenig, T. Douillard, J. Chevalier, F. Amiard, M. Lamy De La Chapelle, S. Le Goff, et al., Intraoral low-temperature degradation of monolithic zirconia dental prostheses: 5-year results of a prospective clinical study with ex vivo monitoring, Dent. Mater. 40 (2024) 198–209, https://doi.org/10.1016/j.dental.2023.11.008.

[18] J. Chevalier, L. Gremillard, 1.6 zirconia as a biomaterial☆, in: P. Ducheyne (Ed.), Compr. Biomater. II, Elsevier, Oxford, 2017, pp. 122–144, https://doi.org/10.1016/B978-0-12-803581-8.10245-0.

[19] H.-K. Kim, Optical and mechanical properties of highly translucent dental zirconia, Materials 13 (2020) 3395, https://doi.org/10.3390/ma13153395.

[20] F. Zhang, M. Inokoshi, M. Batuk, J. Hadermann, I. Naert, B. Van Meerbeek, et al., Strength, toughness and aging stability of highly-translucent Y-TZP ceramics for dental restorations, Dent. Mater. 32 (2016) e327–e337, https://doi.org/10.1016/j.dental.2016.09.025.

[21] E.B. Benalcázar-Jalkh, E.T.P. Bergamo, T.M.B. Campos, P.G. Coelho, I. Sailer, S. Yamaguchi, et al., A narrative review on polycrystalline ceramics for dental applications and proposed update of a classification system, Materials 16 (2023) 7541, https://doi.org/10.3390/ma16247541.

[22] T. Strasser, M. Wertz, A. Koenig, T. Koetzsch, M. Rosentritt, Microstructure, composition, and flexural strength of different layers within zirconia materials with strength gradient, Dent. Mater. 39 (2023) 463–468, https://doi.org/10.1016/j.dental.2023.03.012.

[23] S. Vardhaman, M. Borba, M.R. Kaizer, D. Kim, Y. Zhang, Wear behavior and microstructural characterization of translucent multilayer zirconia, Dent. Mater. 36 (2020) 1407–1417, https://doi.org/10.1016/j.dental.2020.08.015.

[24] Q.-L. Li, Y.-Y. Jiang, Y.-R. Wei, M.V. Swain, M.-F. Yao, D.-S. Li, et al., The influence of yttria content on the microstructure, phase stability and mechanical properties of dental zirconia, Ceram. Int 48 (2022) 5361–5368, https://doi.org/10.1016/j.ceramint.2021.11.079.

[25] R.S. Uwanyuze, S. Ramesh, M.K. King, N. Lawson, M.K. Mahapatra, Mechanical properties, translucency, and low temperature degradation (LTD) of yttria (3–6 mol%) stabilized zirconia, Ceram. Int 47 (2021) 15868–15874, https://doi.org/10.1016/j.ceramint.2021.02.161.

[26] E.N.S. de Araújo-Júnior, E.T.P. Bergamo, T.M.B. Campos, E.B. Benalcázar Jalkh, A. C.O. Lopes, K.N. Monteiro, et al., Hydrothermal degradation methods affect the properties and phase transformation depth of translucent zirconia, J. Mech. Behav. Biomed. Mater. 112 (2020) 104021, https://doi.org/10.1016/j.jmbbm.2020.104021.

[27] G.K.R. Pereira, A.B. Venturini, T. Silvestri, K.S. Dapieve, A.F. Montagner, F.Z. M. Soares, et al., Low-temperature degradation of Y-TZP ceramics: a systematic review and meta-analysis, J. Mech. Behav. Biomed. Mater. 55 (2016) 151–163, https://doi.org/10.1016/j.jmbbm.2015.10.017.

[28] H. Toraya, M. Yoshimura, S. Somiya, Calibration curve for quantitative analysis of the monoclinic-tetragonal ZrO2 system by X-ray diffraction, J. Am. Ceram. Soc. 67 (1984) C-119–C–121, https://doi.org/10.1111/j.1151-2916.1984.tb19715.x.

[29] K. Nakamura, S. Shishido, R. Inagaki, T. Kanno, S. Barkarmo, P. Svanborg, et al., Critical evaluations on the crystallographic properties of translucent dental zirconia ceramics stabilized with 3–6 mol% yttria, Dent. Mater. Publ. Acad. Dent. Mater. 40 (2024) 1425–1451, https://doi.org/10.1016/j.dental.2024.06.027.

[30] D.R. Clarke, F. Adar, Measurement of the crystallographically transformed zone produced by fracture in ceramics containing tetragonal zirconia, J. Am. Ceram. Soc. 65 (1982) 284–288, https://doi.org/10.1111/j.1151-2916.1982.tb10445.x.

[31] ASTM, ASTM E112-13. Test Methods for Determining Average Grain Size 2013. https://doi.org/10.1520/E0112-12.

[32] M.I. Mendelson, Average grain size in polycrystalline ceramics, J. Am. Ceram. Soc. 52 (1969) 443–446, https://doi.org/10.1111/j.1151-2916.1969.tb11975.x.

[33] J.C. Wurst, J.A. Nelson, Lineal intercept technique for measuring grain size in two-phase polycrystalline ceramics, J. Am. Ceram. Soc. 55 (1972) 109, https://doi.org/10.1111/j.1151-2916.1972.tb11224.x.

[34] G. Sharma, W. Wu, E.N. Dalal, The CIEDE2000 color-difference formula: Implementation notes, supplementary test data, and mathematical observations, Color Res Appl. 30 (2005) 21–30, https://doi.org/10.1002/col.20070.

[35] R.D. Paravina, R. Ghinea, L.J. Herrera, A.D. Bona, C. Igiel, M. Linninger, et al., Color difference thresholds in dentistry: color difference thresholds, J. Esthet. Restor. Dent. 27 (S1) (2015) 9, https://doi.org/10.1111/jerd.12149.

[36] C.À.M. Volpato, P.F. Cesar, M.A. Bottıno, Influence of accelerated aging on the color stability of dental zirconia: influence of aging on the color of zirconia, J. Esthet. Restor. Dent. 28 (2016) 304–312, https://doi.org/10.1111/jerd.12239.

[37] CIE Publication “Colorimetry” 2004;No.15.

[38] M. Amaral, L.F. Valandro, M.A. Bottino, R.O.A. Souza, Low-temperature degradation of a Y-TZP ceramic after surface treatments, J. Biomed. Mater. Res B Appl. Biomater. 101 (2013) 1387–1392, https://doi.org/10.1002/jbm.b.32957.

[39] L.F. Guilardi, G.K.R. Pereira, V.F. Wandscher, M.P. Rippe, L.F. Valandro, Mechanical behavior of yttria-stabilized tetragonal zirconia polycrystal: effects of different aging regimens, Braz. Oral. Res 31 (2017) e94, https://doi.org/10.1590/1807-3107bor-2017.vol31.0094.

[40] E.O. Sousa, T.M.B. Campos, E.T.P. Bergamo, L.M.M. Alves, E.B. Benalcazar-Jalkh, M.M. Marun, et al., Nanomechanical and microstructural properties of experimental bilayered zirconia ceramics after hydrothermal aging, Ceram. Int (2024) S0272884224028979, https://doi.org/10.1016/j.ceramint.2024.07.026.

[41] C.H. Lim, S. Vardhaman, N. Reddy, Y. Zhang, Composition, processing, and properties of biphasic zirconia bioceramics: relationship to competing strength and optical properties, Ceram. Int 48 (2022) 17095–17103, https://doi.org/10.1016/j.ceramint.2022.02.265.

[42] G.K.R. Pereira, C. Muller, V.F. Wandscher, M.P. Rippe, C.J. Kleverlaan, L. F. Valandro, Comparison of different low-temperature aging protocols: its effects on the mechanical behavior of Y-TZP ceramics, J. Mech. Behav. Biomed. Mater. 60 (2016) 324–330, https://doi.org/10.1016/j.jmbbm.2016.02.017.

[43] J. Chevalier, L. Gremillard, S. Deville, Low-temperature degradation of zirconia and implications for biomedical implants, Annu Rev. Mater. Res 37 (2007) 1–32, https://doi.org/10.1146/annurev.matsci.37.052506.084250.

[44] E.T.P. Bergamo, T.M.B. Campos, A.C.O. Lopes, K.B. Cardoso, M.V.R. Gouvea, E.N. S. de Araújo-Júnior, et al., Hydrothermal aging affects the three-dimensional fit and fatigue lifetime of zirconia abutments, J. Mech. Behav. Biomed. Mater. 124 (2021) 104832, https://doi.org/10.1016/j.jmbbm.2021.104832.

[45] M.A.P. Borges, M.R. Alves, H.E.S. Dos Santos, M.J. Dos Anjos, C.N. Elias, Oral degradation of Y-TZP ceramics, Ceram. Int 45 (2019) 9955–9961, https://doi.org/10.1016/j.ceramint.2019.02.038.

[46] N. Kolakarnprasert, M.R. Kaizer, D.K. Kim, Y. Zhang, New multi-layered zirconias: Composition, microstructure and translucency, Dent. Mater. 35 (2019) 797–806, https://doi.org/10.1016/j.dental.2019.02.017.

[47] E.O. Sousa, L.M.M. Alves, T.M.B. Campos, E.T.P. Bergamo, E.B. Benalcazar-Jalkh, M.M. Marun, et al., Experimental bilayer zirconia systems after aging: Mechanical, optical, and microstructural characterization, S0109564124003622, Dent. Mater. (2025), https://doi.org/10.1016/j.dental.2024.12.012.

[48] P.F. Cesar, R.B.D.P. Miranda, K.F. Santos, S.S. Scherrer, Y. Zhang, Recent advances in dental zirconia: 15 years of material and processing evolution, Dent. Mater. 40 (2024) 824–836, https://doi.org/10.1016/j.dental.2024.02.026.

[49] R.M. Pereira, T. Moreira Bastos Campos, E. Augusto Bonfante, G. Patrocínio Thim, A comparative study of mechanical properties of yttria stabilized zirconia monolithic and bilayer configuration for dental application, J. Mech. Behav. Biomed. Mater. 148 (2023) 106160, https://doi.org/10.1016/j.jmbbm.2023.106160.

[50] E.B. Benalcázar-Jalkh, T.M.B. Campos, C. Dos Santos, L.M.M. Alves, L.F. Carvalho, E.T.P. Bergamo, et al., Novel bilayered zirconia systems using recycled 3Y-TZP for dental applications, S0109564124003634, Dent. Mater. (2025), https://doi.org/10.1016/j.dental.2024.12.013.

[51] R.C. Garvie, P.S. Nicholson, Phase analysis in zirconia systems, J. Am. Ceram. Soc. 55 (1972) 303–305, https://doi.org/10.1111/j.1151-2916.1972.tb11290.x.

[52] Y. Zhang, Making yttria-stabilized tetragonal zirconia translucent, Dent. Mater. 30 (2014) 1195–1203, https://doi.org/10.1016/j.dental.2014.08.375.

[53] C. Liu, A. Eser, T. Albrecht, V. Stournari, M. Felder, S. Heintze, et al., Strength characterization and lifetime prediction of dental ceramic materials, Dent. Mater. 37 (2021) 94–105, https://doi.org/10.1016/j.dental.2020.10.015.

[54] M. Wendler, M.R. Kaizer, R. Belli, U. Lohbauer, Y. Zhang, Sliding contact wear and subsurface damage of CAD/CAM materials against zirconia, Dent. Mater. 36 (2020) 387–401, https://doi.org/10.1016/j.dental.2020.01.015.

[55] M.R. Kaizer, N. Kolakarnprasert, C. Rodrigues, H. Chai, Y. Zhang, Probing the interfacial strength of novel multi-layer zirconias, Dent. Mater. 36 (2020) 60–67, https://doi.org/10.1016/j.dental.2019.10.008.